Fault Imaging using the Fault Flooding Method

Ahmed Metwally[1], Maximillian Kosmicki[1]
[1]Earth Science and Engineering Department, King Abdullah University of Science and Technology (KAUST).

ABSTRACT

A novel technique was used to image near vertical fault surfaces on synthetic data as well as on field data from a previous near surface seismic survey at the Gulf of Aqaba in Saudi Arabia. The technique used was the 'fault flooding' method, in which a cross correlation was performed on observed refraction arrivals and synthetic refraction arrivals generated from a model simulating a subsurface with no fault. The product of that cross correlation is migrated along ray paths determined by the velocity of the respective models and the location where the two events intersect is the fault scarp. The method was successfully demonstrated on synthetic data from a vertical and titled fault as well as from raw data from the Gulf of Aqaba, where it located two faults previously interpretted from traveltime tomography.

INTRODUCTION

Seismic migration methods typically perform poorly in the location of steeply dipping events such as normal faults and beds dipping at the near vertical. Being able to qualify the dip of faults is very important for understanding the seismogenic properties of the fault system and in turn the implications that have for engineering geology. In order to better locate fault parameters with seismic surveying, the fault flooding method is used to try to directly find the slope and spatial coordinates of faulted portions of the near surface.

THEORY

The general theory behind the fault flooding method pertains to the use of cross correlations on seismic data. A cross correlation has the effect of removing the common ray path terms between two arrivals at a pair of geophones. For the purpose of illustration, let there be a two layer earth model with a fault and a two layer earth model with no fault. A refraction ray path for both models would be identical up until the upgoing head wave for the faulted model reaches the fault and starts traveling with a new velocity. The non-faulted model would still travel with the prior velocity. Once past the point of interception along the fault, the two models diverge with one ray path bending away from the fault (if the velocity on the other side is higher) while the other ray path maintains the same angle and intercepts a earlier receiver. An illustration of this can be seen in the lower panels of Figure 1.

The cross correlation of these two ray paths will leave two events: the non-faulted model traveling past the fault surface at the velocity of the left hand side of the fault and the faulted model traveling at the velocity of the right hand side of the fault. The general idea behind the fault flooding algorithm is that these events can be migrated with there respective velocities back to the fault scarp, the point of their common intersection after the cross correlation. The general workflow for performing the fault flooding method is as follows:

1. Identify and isolate refraction arrivals in data
2. Generate synthetic data for a non-faulted scenario and isolate refraction arrivals
3. Perform a cross correlation of the virtual refractions (non-faulted) and the observed refractions (faulted)
4. Migrate the product of the cross correlation to the fault scarp.

Refraction migration is used to delineate the location of refracting interfaces (Hill, 1987; Zhang, 2006; and many

others). The diffraction-stack migration equation for refractions is:

$$m(x) = \sum_{\omega}\sum_{r}\sum_{s} D(g,s,\omega)e^{-i\omega(\tau_{sx}+\tau_{xg})}, \quad (1)$$

The observed $D(g,s,\omega)_{obs}$ and virtual $D(g,s,\omega)_{virt}$ refraction data on the surface can be mathematically represented by:

$$\begin{aligned} D(g,s,\omega)_{obs} &= e^{i\omega(\tau^1_{sx_o}+\tau^2_{x_o g})}; \\ D(g',s,\omega)_{virt} &= e^{i\omega(\tau^1_{sx_o}+\tau^1_{x_o g'})}, \end{aligned} \quad (2)$$

where $'$ is the virtual geophone location associated with the observed data recorded at , and the superscripts in the traveltimes indicate the traveltime in the medium with velocity v_1 or v_2. The location $_o$ indicates the common intersection point of the observed and virtual refraction rays at the fault.

Correlating the recorded and virtual traces gives the operator Φ:

$$\begin{aligned} \Phi(g,g',s,\omega) &= D(g,s,\omega)_{obs} D(g',s,\omega)^*_{virt} \\ &= e^{i\omega(\tau^2_{x_o g}-\tau^1_{x_o g'})}. \end{aligned} \quad (3)$$

The migration kernel that cancels the phase of the equation 3 data at $_o$ is $e^{-i\omega(\tau^2_{xg}-\tau^1_{xg'})}$ so the migration equation for imaging the fault is given by:

$$m(x) = \sum_{\omega}\sum_{s}\sum_{g}\sum_{g'} \Phi(g,g',s,\omega)e^{-i\omega(\tau^2_{xg}-\tau^1_{xg'})}. \quad (4)$$

Equation 4 is equivalent to interferometrically detecting the location of a point source (Schuster, 2009) at $_o$, except now the source is at the location of the fault boundary.

Refraction migration is restricted to the imaging of refraction interfaces, not the imaging of fault boundaries. For example, the head wave raypath (denoted as the actual black ray in Figure 1b) abruptly changes its angle of propagation across the vertical fault, and is characterized by a sharp *inflection* in the slope of the observed refractions. Therefore, the refraction ray does not refract along the fault scarp so the scarp will not be imaged by refraction migration. The key identifier of a near-surface fault is that the inflection's trace position **A** does not change with source position even if the source is on the opposite side of the scarp (Schuster 2015).

SYNTHETIC EXAMPLES

Vertical Fault Model

A synthetic data set (Figure 3) is generated using a finite-difference solution to the 2D acoustic wave equation for the velocity model represented by (Figure 2). A total of

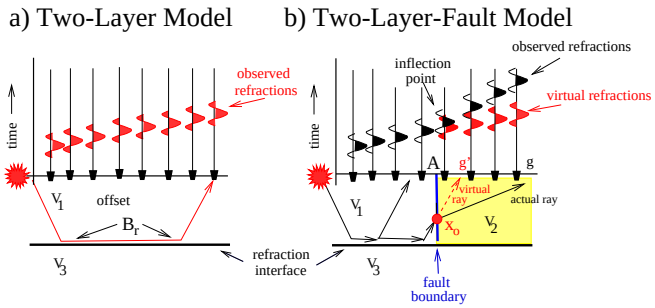

Figure 1: Common shot gathers for the a) two-layer and b) two-layer-fault models. The red virtual refractions in b) are obtained by creating the red arrivals (with $1/v_1$ slope) to the right of the inflection point at **A**. Here, $v_2 < v_1 < v_3$. The position $_o$ must be at the fault if the backprojected virtual and actual rays intersect at $_o$ *and* their arrival times agree with one another (schuster 2015).

150 common shot gathers (CSG) are computed for a set of 150 receivers with 30 meters as the spacing for both the shot and receiver intervals. A synthetic data set (Figure 5) is generated using the same technique with the same survey geometry for the non-faulted velocity model (Figure 4) in order to get the virtual data set (non-faulted).

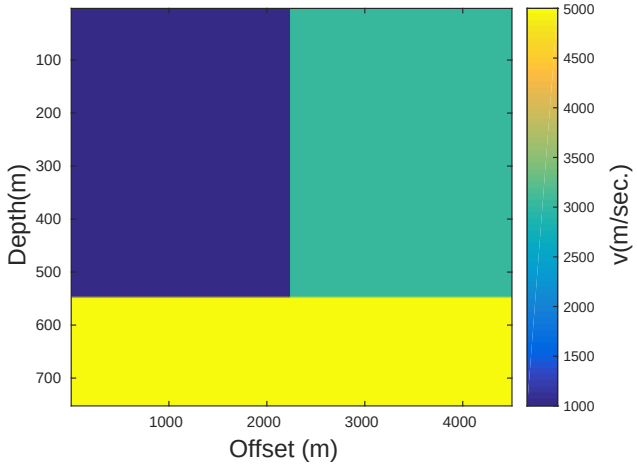

Figure 2: Velocity model for a vertical fault used to generate the observed data.

Then from the observed and the virtual data sets, the refractions are isolated to get the observed refraction arrivals (Figure 6) and the virtual refraction arrivals (Figure 7). The refractions from the observed and the virtual datasets will then be cross correlated together to get the correlated image (Figure 8) on which the migration kernel will be applied to get the final migration image of the fault (Figure 9). The result can be seen in Figure 9.

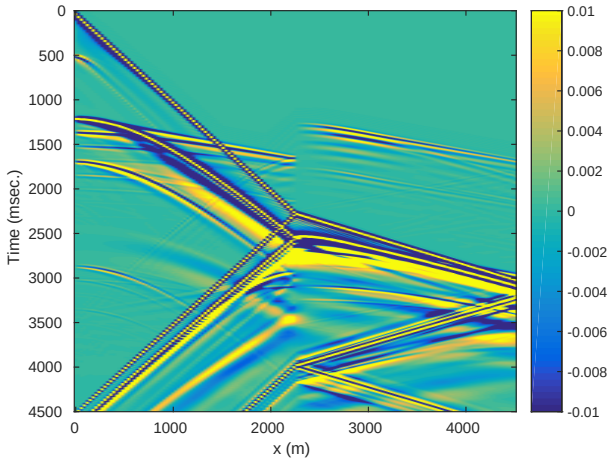

Figure 3: Synthetic data set generated from the vertical fault example.

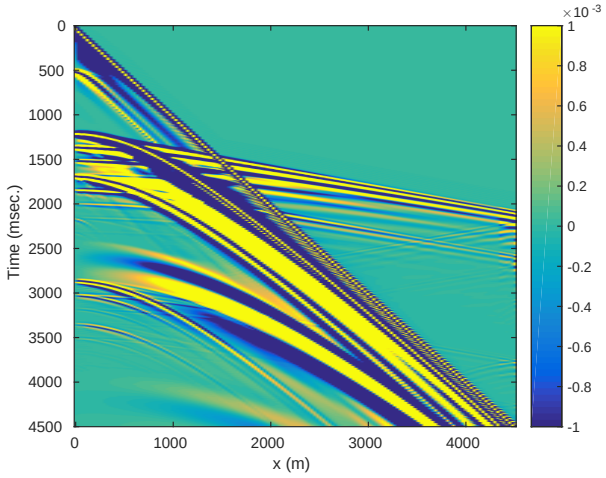

Figure 5: Synthetic data set generated from the non-faulted velocity model (virtual data).

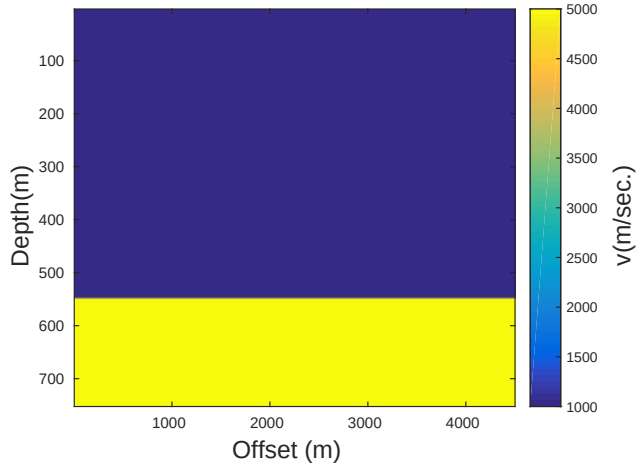

Figure 4: Velocity model for a non-faulted example to generate the virtual data.

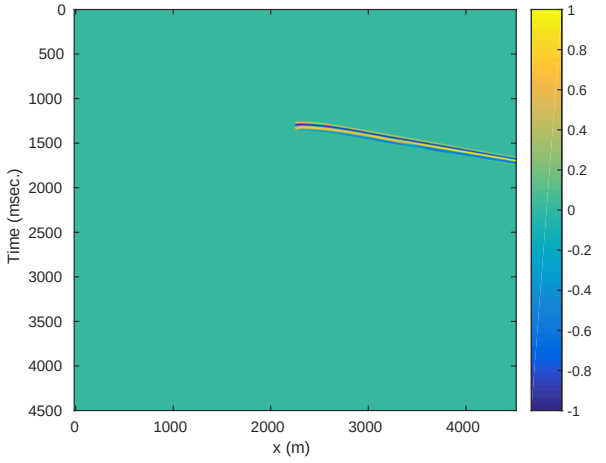

Figure 6: Isolated refractions from the observed synthetic data.

Tilted fault model

In a process similar to teh previous example, a synthetic data set (Figure 11) is generated using a finite-difference solution to the 2D acoustic wave equation for the velocity model represented by (Figure 10). A total of 150 common shot gathers (CSG) are computed for 150 receivers with 30 meters as the shot and receiver interval. A synthetic data set (Figure 5) is generated using the same technique and with the same geometry for the non-faulted velocity model (Figure 4) to get the virtual data set (non-faulted).

Then from the observed and the virtual data sets the refractions are isolated to get the observed refraction arrivals (Figure 12) and the virtual refraction arrivals (Figure 7). Those refractions from the observed and the virtual data sets are then cross correlated together to get the correlated image (Figure 13) on which the migration kernel will be applied to get the final migration image of the fault (Figure 9).

FIELD DATA EXAMPLE

The same general algorithm, with a few modifications, was applied on field data collected from the Gulf of Aqaba in a 2014 survey. The seismic data set was collected to map the subsurface structure of the region and detect faulting in the area (Figure 15). A total of 120 common shot gathers were collected. Each shot gather had 120 traces at equal shot and receiver intervals of 2.5 meters. The total length of the profile is 297.5 meters. Data was recorded using a 1 ms sampling interval for a total recording time of 0.3 seconds. A 200 lb weight drop was used as the seismic source, with 10 to 15 stacks at each shot location.

In order to generate the synthetic data, the observed CSG's were modified to resemble the refraction arrivals of the non-faulted model by flattening the kinks associated

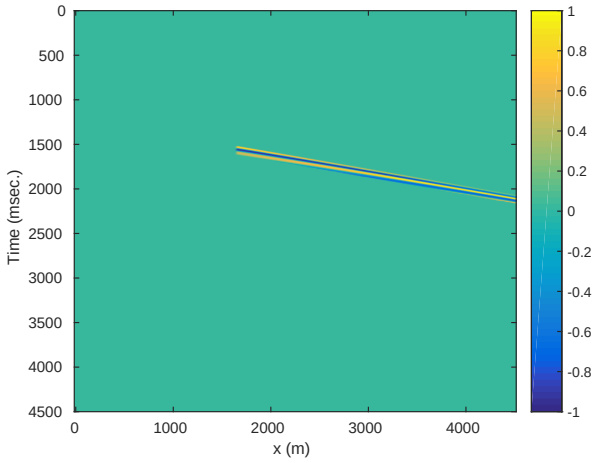

Figure 7: Isolated refractions from the virtual synthetic data.

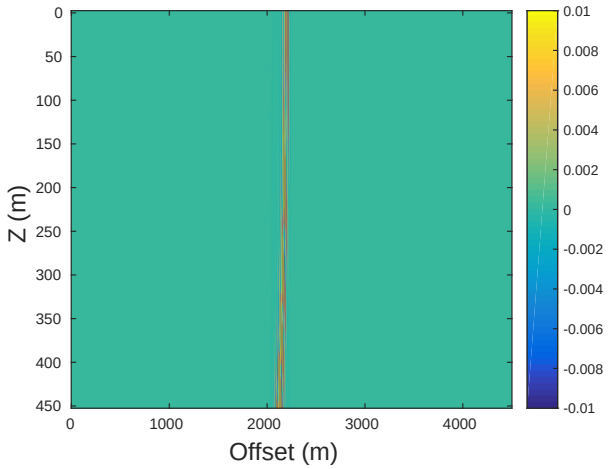

Figure 9: Final migration image showing the fault in the same location as the velocity model.

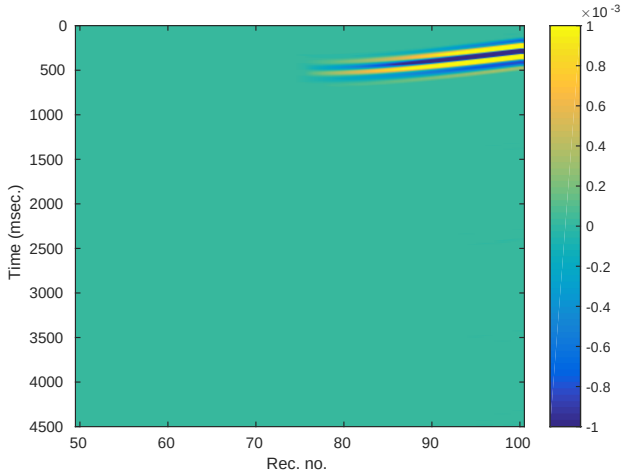

Figure 8: Correlated data by cross correlating the observed and virtual refractions.

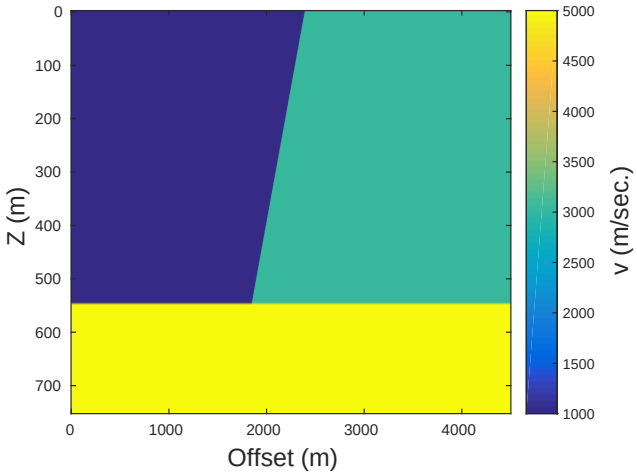

Figure 10: Velocity model for a tilted fault example to generate the observed data.

with the normal faults. This was done through shifting the kinked areas to be in line with the slope of the other first arrivals. A comparison of the two methods can be seen in (Figure 16) and (Figure 17). Muting was also performed in order to isolate the refraction arrivals (Figures 18, 19) and the resulting cross correlation image of the data can be seen in (Figure 20). After migration, the image representing the possible locations of the faults in the Aqaba region can be seen in (Figure 21).

LIMITATIONS

The fault flooding method is not without limitations. Primarily the method requires a sharp velocity difference across a vertical fault scarp, however many near surface faults will be faults that occur within a single geologic layer that has negligible change in velocity across the fault interface. Strike slip faults for example will most likely not be able to be imaged with this method as the velocity on both sides of the fault interface are often the same. Geometrically, this method only can truly find the true fault parameters if performed perpendicular to the strike of the fault. Any other orientation will result in obtaining the apparent dip of the fault.

Additionally there exists the possiblilty of mispicking refraction arrivals from deeper layers or non fault related velocity changes in the refraction arrivals as kinks caused by near vertical faults. The intersection of refraction arrivals from deeper layers and the kink that would be associated with a fault with a high-to-low velocity transition would look the same.

CONCLUSIONS

The synthetic data examples indicate that on the conceptual and theoretical level, the fault flooding method is a

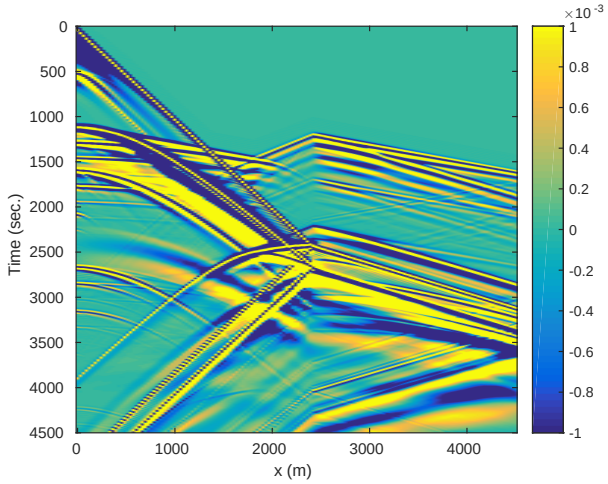

Figure 11: Synthetic data set generated from the tilted fault example.

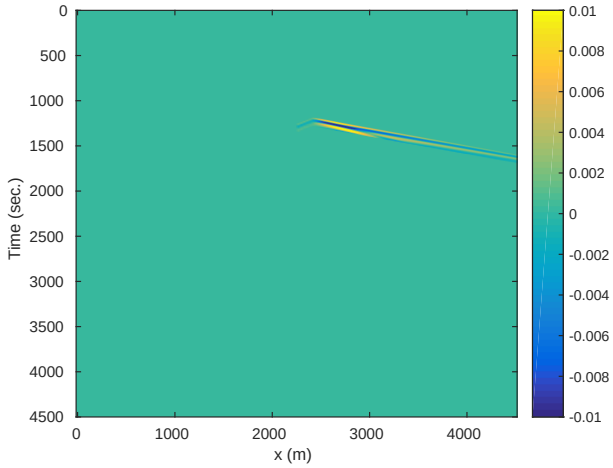

Figure 12: Isolated refractions from the observed synthetic data for the tilted fault model.

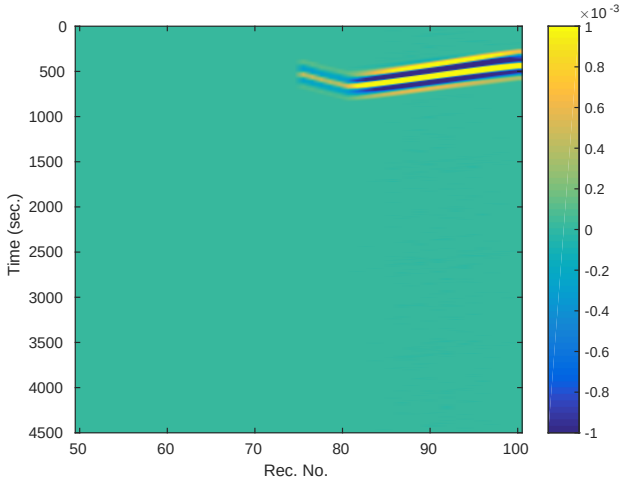

Figure 13: Correlated data by cross correlating the observed (from the tilted fault model) and virtual refractions.

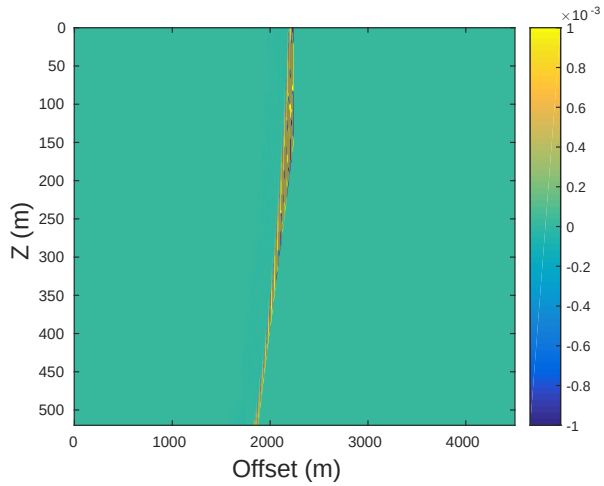

Figure 14: Final migration image showing the tilted fault in the same location as the velocity model.

success in migrating seismic data to the fault surface. It is worth noting that the location of the fault becomes less constrained as depth increases in both the dipping and vertical scenarios. Similarly the fault flooding method passes the field data test by successfully locating two faults found previously through travel time tomography. The result is more diffuse from the synthetic trials, but it reflects the less percise nature of fieldwork as compared to theory.

The fault flooding method is a potentially powerful tool in the determination of the location of near verical faults. Assuming that there are clear refraction arrivals and kinks are visible in the section, this algorithm allows for a better discernment of the subsurfcae extents of the fault. This method is able to resolve both near vertical and vertical faults. However, this method will not resolve faults that are not bounded by some transition in velocity across the interface and care should be taken to isolate only events caused by near surface faulting and avoiding mislabeling non-fault related events such as multiple refractor transitions as faults.

REFERENCES

[h!] Hanafy, S., SEG 2014, Imaging Normal Faults in Alluvial Fans using Geophysical Techniques: Field Example from the Coast of Gulf of Aqaba, Saudi Arabia.

Hill, R., 1987, Downward continuation of refracted arrivals to determine shallow structures: Geophysics, **52**, 1188-1198.

Schuster, G., 2009, Seismic Interferometry: Cambridge Press.

Schuster,G., 2015, Imaging of Near-Surface Faults by Fault Flooding and Refraction Migration.

Sun, H. and G. T. Schuster, 2001, 2-D wavepath migra-

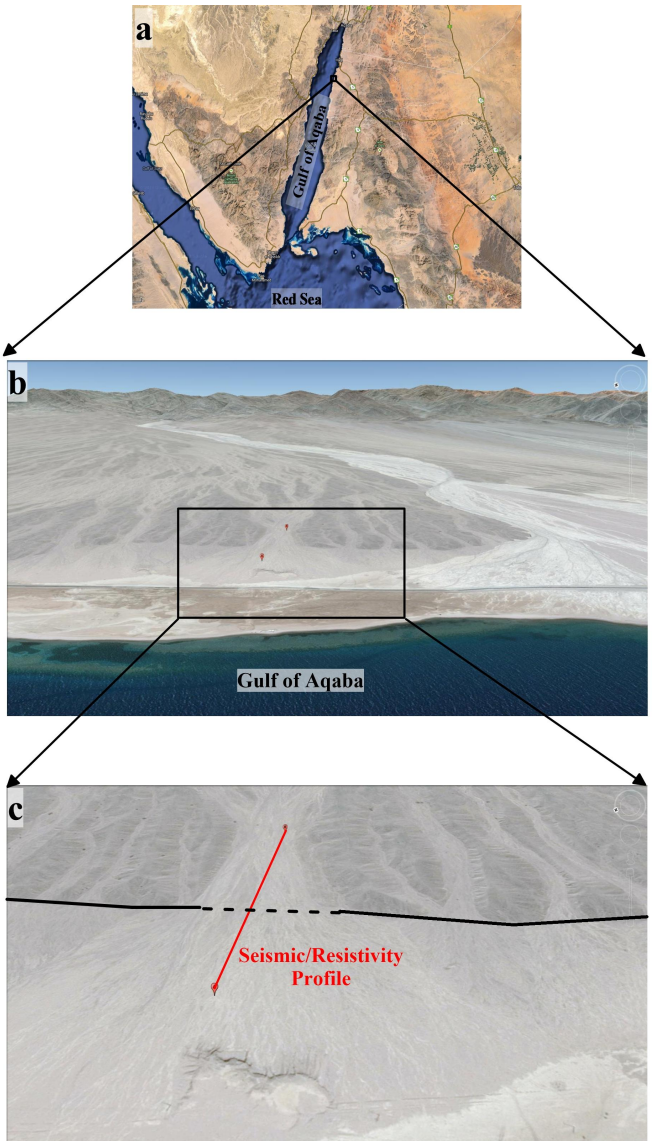

Figure 15: a)A map showing the Gulf of Aqaba. b)A photo showing the shore line with the start and end of the survey line shown in red dots c) Zoomed picture showing the location of the survey line.

tion: Geophysics: **5**, 1528–1537.

Zhang, J., 2006, Refraction migration: imaging multiple refractors automatically: Expanded Abstract, SEG 71st Annual Meeting in New Orleans, Louisiana, 2426-2430.

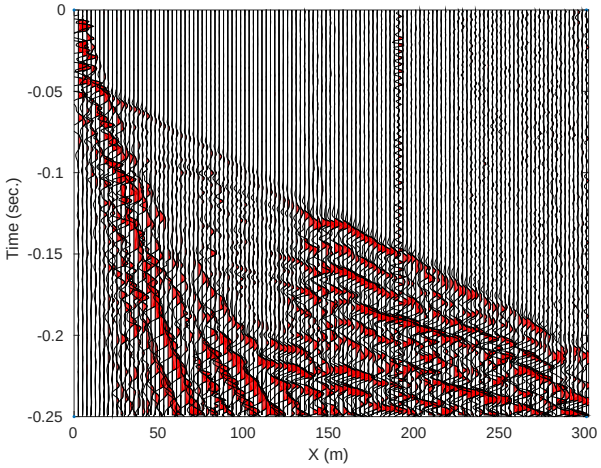

Figure 16: CSG of the first shot, the 'kink' associated with the fault is seen as the two dips in the refraction arrivals.

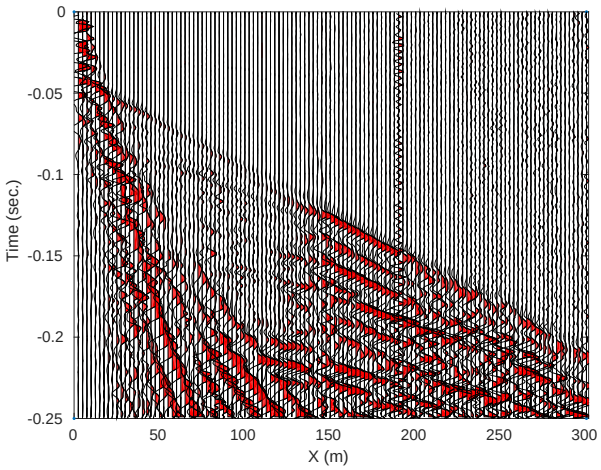

Figure 17: Virtual CSG of the first shot, the kinks that were in the observed CSG have been removed.

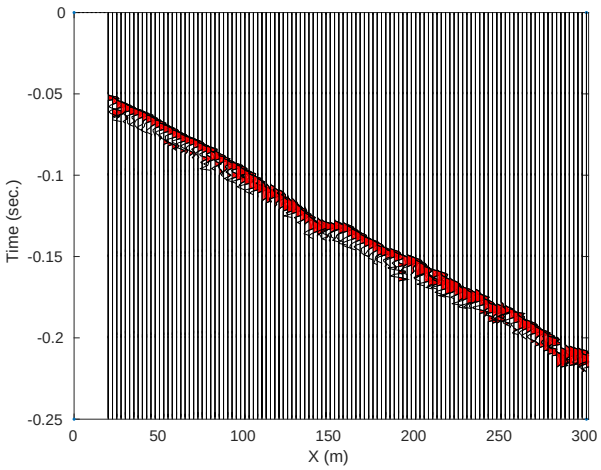

Figure 18: Muted CSG of the first shot.

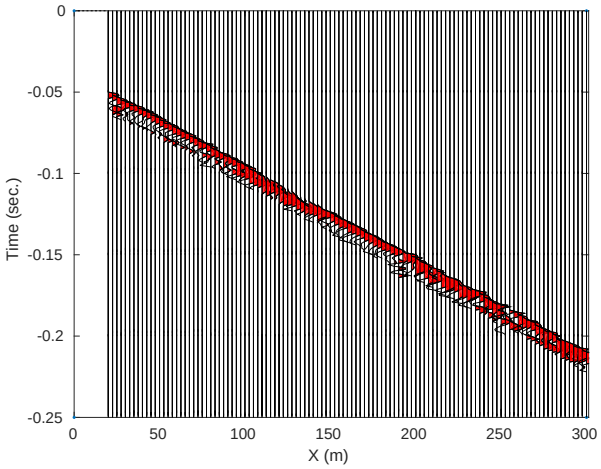

Figure 19: Muted Virtual CSG of the first shot.

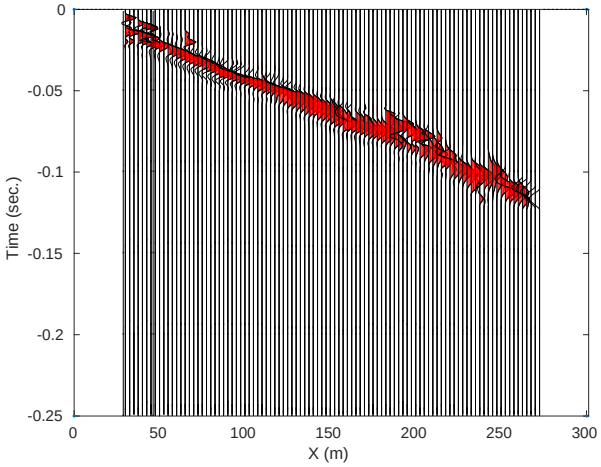

Figure 20: Image of the cross correlation of the observed and virtual data.

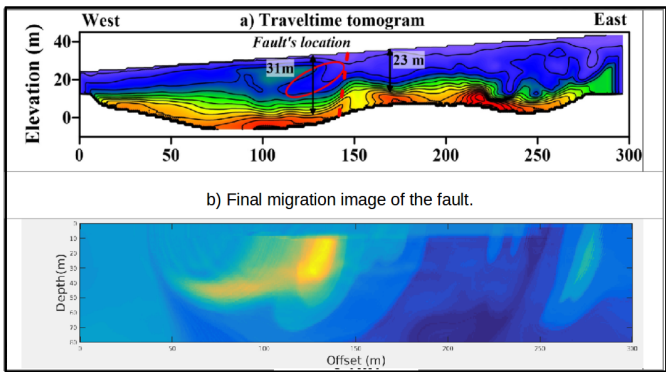

Figure 21: a) Results obtained by Hanafy, 2014 b) Final migration of the Gulf of Aqaba Data showing the faults.